

DEVELOPING A SMART FAÇADE SYSTEM CONTROLLER FOR WIND-INDUCED VIBRATION MITIGATION IN TALL BUILDINGS

Khalid M. Abdelaziz

PhD Student

Dept. of Mechanical and Nuclear Engineering
 Kansas State University
 Manhattan, Kansas, USA

Jared D. Hobeck

Assistant Professor

Dept. of Mechanical and Nuclear Engineering
 Kansas State University
 Manhattan, Kansas, USA

ABSTRACT

Tall and slender buildings often endure disturbances resulting from winds composed of various mean and fluctuating velocities. These disturbances result in discomfort for the occupants as well as accelerated fatigue life cycles and premature fatigue failures in the building. This work presents the development of a smart morphing façade (Smorphacade) system that dynamically alters a buildings' external shape or texture to minimize the effect of wind-induced vibrations on the building. The Smorphacade system is represented in this work by a series of plates that vary their orientation by means of a central controller module. To validate the simulation, a simple NACA0012 airfoil is simulated in a stream of air at a Reynolds number (RE) of 2 million. The pressure and viscous force profiles are captured to plot the variation of the lift force for different angles of attack that are then validated using published experimental airfoil data. After validation, the airfoil is attached to a linear spring-damper combination and is allowed to translate vertically without rotation according to the force profile captured from the surrounding air stream. A PID controller is developed to equilibrate the vertical position of the airfoil by altering its angle of attack. The model and its utility functions are implemented as an OpenFOAM® module (MSLSolid). Thereafter, the model is expanded to handle a planar case of a building floor carrying 4 controllable plates. The forces on the building profile are summed at the centroid of the building and the windward rigid body motion of the floor is estimated by reflecting the horizontal force component on a Finite Element (FE) model of the building. The time series information of the force acting on the building and the resulting oscillations are captured for exhaustive combinations of the plate angles. This data is used to build a lookup table that gives the best plate configuration for a given wind condition. A controller operates in real-time by searching the lookup table using readings of the wind condition. Preliminary results show a 94% reduction in the amplitudes of wind-induced vibrations.

1. INTRODUCTION

Buildings are becoming taller and more lightweight as a result of the developments in building designs and construction materials [1]. These materials have become lighter, more flexible and more absorbent of energy resulting from wind-induced vibrations [2] because of their lower damping capacity [1, 3]. In several cases, structural damage or even collapse resulted from vibrations occurring at low wind speeds even if the structure was designed for much higher wind speeds (e.g., Tacoma bridge 1940) [4, 5]. This can be explained by the vortex formations in the wake of the building due to the separation of flow around the building. These vortices cause fluctuations in the forces affecting the building which excites it at the vortex system frequencies which could be close to the its natural frequencies [1]. Additionally, the occurrence of wind gusts either in speed or direction contributes to the severity of these oscillations in an inevitable way [6, 7]. Façade components and building partitions may also suffer from damage and require more frequent maintenance as a result [3, 8]. Finally, occupant discomfort is another downside of such oscillations and the perception of accelerations resulting from wind is evident in many cases [6, 8]. The development of systems to mitigate wind-induced vibrations has drawn a lot of research interest in recent years because of these concerns.

Tuned Mass Damper (TMD) systems are one of the solutions that has been thoroughly analyzed and tested in various deployments [9]. It involves hanging a large mass from the building like a pendulum and attaching it to a set of dampers. By tuning the pendulum system to absorb a large proportion of the vibration energy from the building, the amplitudes of such vibrations can be reduced considerably. Another similar approach is the Tuned Liquid Damper (TLD) system [3, 10] where a rigid water tank is placed on top of the building so as the sloshing motion of the water will absorb the vibration energy. TLDs operate more efficiently at higher amplitudes [10], and require considerable roof space. Therefore, various

enhancements and modifications were considered to improve their efficiency [11, 12]. However, the mass of both systems is often high and they generally consume space at upper floors where real estate is most expensive. Also, they are usually tuned for white noise wind disregarding gusts and dominant vortex frequencies [10].

Artificial Neural Networks (ANN), inspired by the human brain [13], were shown to successfully perform cognitive tasks that are usually performed by humans like object, speech and handwriting recognition [14, 15]. Special ANN designs were also shown by Kim *et al.* [16] to predict the behavior of nonlinear hysteretic systems including structural response to earthquakes. Given a bluff body (such as a building) in a natural fluid flow environment, the exact vortex formations around the building along with their resulting forces and vibrations are not obviously predictable. ANNs could be very effective at predicting wind-induced vibration while *learning* from the typical response of the building in its natural dynamic environment.

This work proposes a novel approach to address wind-induced vibrations by altering the vortex system frequencies and formation locations. Different wind speeds and directions will cause different vortex systems to be created. Therefore, the façade of the building is to be constructed as a set of movable louvers or plates. Measurements of the speed of the wind attacking the building are input to a controller module that changes the louver orientations to generate desirable vortex shedding characteristics and hence reduce the amplitude of building vibrations. Fluid-solid-interaction (FSI) simulations are utilized to establish correlation between wind speed and direction, the generated vortex system and the vibration amplitudes. Fluid flow simulations for various plate orientations, wind speeds and directions estimate the forces that affect the building for each time step. These forces are reflected on a FE model of the building to estimate the time step response of the building and present position and velocity boundary conditions to the fluid domain accordingly. Because of the large number of plates and possible wind load conditions, it is impractical to run simulations for every possible configuration. Therefore, the data collected in this work is used to teach an ANN setup that predicts the optimum plate configuration for a given wind condition. In wind tunnel experiments or even after deployment, the ANN could still be learning at a faster pace (i.e. not limited by computational time) which will improve its performance over time. Additionally, the erection of new buildings in the vicinity or changes to the structure of the building could affect the typical wind profiles, and the use of the ANN will enable the system to adapt to such changes.

Section 2 of this work discusses the mathematical models involved in the simulations as well as the simulation procedures. Section 3 presents the NACA0012 wing case for verification of the simulation results as well as for illustrating the plate motor controller assumptions. Section 4 discusses the studied 4-plate and 20-plate building models, the development of the controller and the created ANN setup suitable for online learning.

2. SIMULATION MODELING

This section presents the mathematical equations that were used to perform the simulations as well as illustrates how the fluid and the solid simulations interact with each other.

2.1 Fluid Model

For the wind speeds considered (less than 10 m/s), air can be assumed to be incompressible [17]. The Reynolds averaged Navier-Stokes (RANS) equations have been used extensively to solve turbulent flows in similar cases in the literature [17]. The RANS form of the momentum equation which governs incompressible fluid flow is given by [18]:

$$\frac{\partial}{\partial t} \rho \bar{U} + \nabla \cdot (\rho \bar{U} \otimes \bar{U}) = \nabla \cdot \bar{\sigma}_{\text{eff}} + \rho g \quad (1)$$

where ρ is the fluid density, \bar{U} is the mean velocity, $\bar{\sigma}_{\text{eff}}$ is the effective Cauchy-Stress tensor [18]. To close the system of equations, The $k - \varepsilon$ turbulence model [19] was used because it is known to be suitable for external flows and because of its stability and low computational cost [20]. The standard form of this model is given as two transport equations [19, 21] :

$$\frac{\partial}{\partial t} (\rho k) + \frac{\partial}{\partial x_i} (\rho k u_i) = \frac{\partial}{\partial x_i} \left[\left(\mu + \frac{\mu_t}{\sigma_k} \right) \frac{\partial k}{\partial x_j} \right] \dots + G_k - \rho \varepsilon \quad (2)$$

$$\frac{\partial}{\partial t} (\rho \varepsilon) + \frac{\partial}{\partial x_i} (\rho \varepsilon u_i) = \frac{\partial}{\partial x_j} \left[\left(\mu + \frac{\mu_t}{\sigma_\varepsilon} \right) \frac{\partial \varepsilon}{\partial x_j} \right] \dots + C_{1\varepsilon} \frac{\varepsilon}{k} G_k - C_{2\varepsilon} \rho \frac{\varepsilon^2}{k} \quad (3)$$

where k is the kinetic energy, ε is its dissipation rate, μ_t is the turbulent viscosity, G_k is the generation of turbulent kinetic energy due to the mean velocity gradients and C_μ , $C_{1\varepsilon}$, $C_{2\varepsilon}$, σ_k , σ_ε are constants of the model. The full model and the constant values are detailed by Cabezón *et al.* [20]. Finally, the continuity equation for incompressible flow gives the divergence-free condition for the velocity U :

$$\frac{\partial U_i}{\partial x_i} = 0 \quad (4)$$

Equations 1-4 are discretized using appropriate schemes for each term on a 2D finite volume mesh created using SALOME® [22]. OpenFOAM® [23] implementation of the PIMPLE (PISO+SIMPLE) [18] algorithm is used for time integration as well as pressure-velocity coupling with a dynamic time step that changes to satisfy a certain value for the Courant number [18]. A Courant number value of 5 showed sufficiently accurate and stable results. ParaView [24] was used throughout this work to visualize and analyze the results.

After the pressure and velocity fields are obtained, MSLSolid performs a summation of the resulting pressure and viscous forces acting on the body (building floor with plates or airfoil) assuming a depth dimension that represents the height of the building floor or the span of the airfoil.

2.2 Solid Model

For tall buildings, bending and torsional deformations of the building as a whole are extensively more significant than relative single-floor deformations. Therefore, the 2D floor embedded in the CFD mesh does not deform and only translates and rotates in the plane as a rigid body according to a cantilever frame model that represents the whole building. The cantilever beam is modeled as a single FE frame element (which could become an arbitrary multi-member frame) whose transient response is given by:

$$M\ddot{X} + C\dot{X} + KX = F \quad (5)$$

where M is the mass matrix of the frame, C is the damping matrix, K is the stiffness matrix, X is a vector of the deflection at the nodal degrees of freedom (DOFs), \dot{X} is the velocity of the deflection, \ddot{X} is the acceleration and F is a vector of the forces extracted from the CFD simulation after being scaled for the depth. Equation 5 is solved using the Householder algorithm for symmetric matrices [26] to provide the instantaneous values of the DOF accelerations \ddot{X} which are integrated using the time step as follows:

$$\dot{X}_{t+\Delta t} = \dot{X}_t + \ddot{X}\Delta t \quad (6)$$

$$X_{t+\Delta t} = X_t + \dot{X}\Delta t \quad (7)$$

with the initial conditions $X(0) = 0$ and $\dot{X}(0) = 0$. MSLSolid synchronizes the time step Δt with the variable step of the CFD simulation automatically. The derivation of the mass matrix M and the stiffness matrix K and their transformation to the global coordinate system are detailed by Bhatti [27]. The damping matrix C is assumed to be a linear combination of M and K (proportional damping) [28]:

$$C = \alpha M + \beta K \quad (8)$$

where α and β are determined by solving the system of equations [28]:

$$\zeta_i = \frac{\alpha}{2\omega_i} + \frac{\beta\omega_i}{2} \quad (9)$$

where ω_i are the undamped natural frequencies for the building and ζ_i are their damping ratios. The damping ratios are assumed as the typical values for buildings [28]. The natural frequencies, however, are calculated by solving the generalized eigenvalue problem:

$$K\phi = \omega^2 M\phi \quad (9)$$

where ϕ is an eigenvector associated with arbitrary ω .

2.3 Fluid-Solid-Interaction

After the instantaneous deflections X are obtained from the solid model, MSLSolid performs the task of moving the body in the

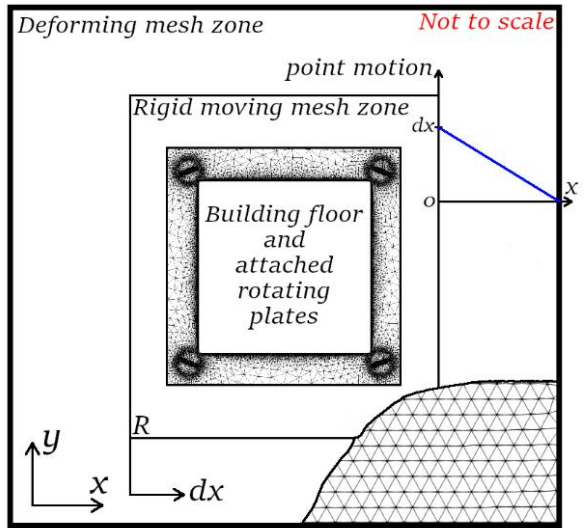


Fig. 1: Motion of mesh points relative to the displacement of the moving region (R)

CFD mesh accordingly. As shown in Fig. 1, a rectangular region R of the mesh surrounding the building and the plates is assumed to have a constant shape so each point of it is moved according to X . The region R typically extends for about 5 times the building width so that the smallest cells in the mesh (adjacent to the solid body) will not endure any volume changes.

The outermost mesh surrounding region R is the only part of the mesh that is allowed to deform. Its cells expand and contract up to the fixed boundary to accommodate translation and rotation of the building. The motion of each node in this deforming mesh region is determined via linear interpolation between nodes on the boundary of R (full motion) and nodes on the outermost boundary of the computational domain (zero motion). All the mesh point motions are performed by utilizing the OpenFOAM dynamic mesh library [29] which adjusts the mass flow through the cell faces automatically, effectively imposing position and velocity boundary conditions on the fluid domain for the next time step. After the motion is performed, the CFD simulation performs its next time step and the process repeats.

The FSI approach presented constitutes an implementation of the widely-used partitioned procedure [25], where the fluid model calculates the forces which the solid model uses to calculate the deflections and generate new position and velocity boundary conditions for the next time step of the fluid model.

3. VALIDATION AND PID CONTROL

A simple NACA0012 airfoil was placed in a rotating mesh bubble as shown in Fig. 2. The mesh has 25,436 nodes and 89,026 elements because it was refined to accurately represent the edge of the airfoil and to match with experimental results. Figure 3 shows a comparison between the generated lift force versus experimental data compiled by Ladson [30] for the purpose of validating the CFD simulation. The figure shows good agreement between experimental and CFD results which

denotes that the rotating mesh interface has a negligible influence on simulation accuracy.

3.1 PID Controller

The airfoil was assumed to have a mass m and was attached to a spring of stiffness k and a damper with a constant c in the vertical direction only, which gives the vertical motion y as:

$$m\ddot{y} + c\dot{y} + ky = L(\alpha) \quad (10)$$

where $L(\alpha)$ is the lift force as a function of the angle of attack α , which is estimated in the design stage from the data compiled by Ladson [30] (see Fig. 3). In the actual simulation, however, $L(\alpha)$ is the vertical component of the force summation around the profile of the airfoil. A PID controller was designed based on the fit in Fig. 3 that moves the airfoil to a reference position y_{ref} by giving a torque command τ to a motor that has its own PID controller to rotate the airfoil. As such, the rotation of the airfoil α was assumed to satisfy:

$$j\ddot{\alpha} + b\dot{\alpha} + h\alpha = \tau \quad (11)$$

where j , b and h are the rotational inertia, viscous damping, and stiffness, respectively. The parameters assumed for both the validation and the PID control are summarized in Table 1. The settling time for the airfoil was 21 seconds and the steady state error was negligible.

4. FOUR-PLATE BUILDING

Figure 4 shows detailed cross-sectional views of the mesh used to simulate a square building with a flat plate attached to each corner. The angle of each plate relative to the x -axis is determined by the controller while the center of mass of each plate moves as if they are fixed to each corner of the building. The building is assumed to be 1×1 m and the domain extends in each direction for 10 m past the boundary of the building. To ease calculations and to obtain preliminary results, the building is assumed to be surrounded by only 4 relatively large plates (0.2 m chord length) rather than a plethora of small louvers or plates as a real façade would typically consist of. To minimize shading effects, the plates are placed at the corners of the building. The plates are assumed to be rigid because the effect of their localized deformations on the building-scale vortex formations is expected to be much smaller than the effect of their rotations. This is especially true in an actual deployment, where the plates would be smaller in comparison to the building size than presented.

The 4-plate mesh has a total of 217,714 nodes and 762,011 elements. As was the case with the NACA0012 airfoil, the plates are placed in rotating mesh bubbles that have interpolation interfaces with the rest of the mesh. Methods used to implement mesh motion, boundary conditions, and mesh interfacing were identical to those used for the airfoil case. For these cases, the wind attacks the building in the positive x direction.

Table 1: Parameters of NACA0012 airfoil case

Parameter	Value	Unit
Mass (m)	5	Kg
Stiffness (k)	4	N/m
Damping (c)	9.8	N.s/m
Wind speed	51.54	m/s
Chord length	0.6	M
RE	2×10^6	-
Mach number	0.15	
Span	0.6	M
Air density (ρ)	1.225	kg/m ³
PID system	0.001, 0, 0.001	-
$y(0)$	0	M
y_{ref}	0.1	M
Rotational b	0.0017	N.m.s ² /rad
Rotational h	1.7×10^{-4}	N.m.s/rad
PID motor	5, 0, 4	
$\alpha(0)$	5	Degree

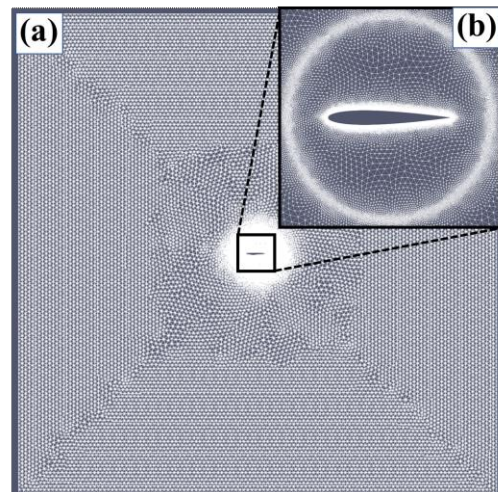


Fig. 2: Computational mesh for the NACA0012 airfoil section
(a) full domain (b) rotating mesh interface detail

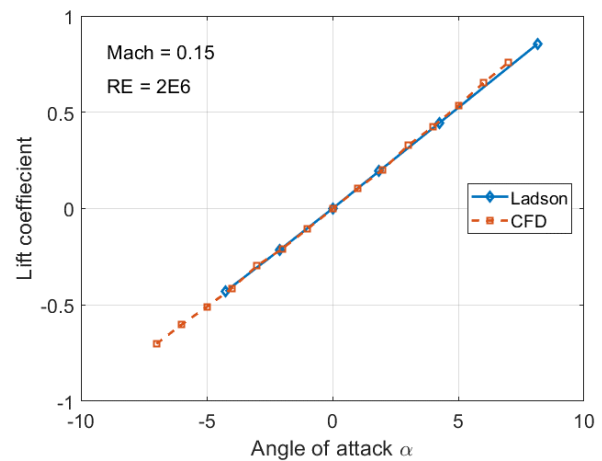


Fig. 3: Validation of the lift coefficient generated from the CFD simulation of the NACA0012 airfoil

4.1 Frequency Matching

As discussed in Section 1, vortex shedding generates a range of frequencies for the forces acting on the building that depends on the geometry and the wind speed, among other factors. To study the feasibility of the proposed system, the cantilever beam representing the building was tuned to generate high-amplitude oscillations for an average wind speed of 5 m/s. To do that, the simulation is run and the time history of the forces and the building deflection are plotted. The frequency of the building oscillation is then adjusted to match that of the forces by changing the material density ρ (to adjust M) and Young's modulus of elasticity E (to adjust K). The purpose of this tuning is to magnify the wind force effects on the building in order to underline the mitigation approach discussed in the following sections. Figure 5 shows a typical history of wind forces and building oscillation after tuning.

4.2 Plate Angle Effect

Having matched the frequencies, it remains to show that changing the plate angles can change the frequency of the wind forces and thus the building oscillation amplitude. This was achieved by running a series of simulations at various constant wind speeds. Plate 3 mirrors plate 1 and plate 4 mirrors plate 2 assuming symmetry relative to the wind direction (positive x , see Fig. 4). This effectively reduces the independent plate angles to α_1 and α_2 , where α_1 is the angle of plates 1 and 3. The simulation issues immediate (zero-time) plate angle changes to study their effect in a shorter simulation as per the following procedure:

1. Run for 10 seconds to let fluid forces stabilize
2. Allow building motion
3. increment α_1 by $\frac{\pi}{8}$
4. Run for t_p seconds
5. Repeat 3, 4 until $\alpha_1 = \frac{7}{8}\pi$
6. Increment α_2 by $\frac{\pi}{8}$
7. Repeat 3, 4, 5, 6 until $\alpha_2 = \frac{7}{8}\pi$
8. Stop the simulation

The time to wait between plate changes t_p is determined manually for each wind speed by observing the time it takes for the transient effects to disappear. In most cases, the transients were negligible after 15 seconds. Seven simulations were performed for a range of wind speeds (5-9 m/s). Each simulation utilized 24 processor cores from the Crunch computational cluster at the Multifunctional Structures Laboratory (MSL) at Kansas State University. Figure 6 and 7 illustrate the wind forces and the corresponding building deflections for a wind speed of 5.5 and 9 m/s, respectively. The figures also show the scaled mean deflection amplitude which is calculated by defining a window of 7 seconds before each plate change and then calculating the moving average of the vibration amplitudes relative to that window for each data point. The choice of 7 seconds was to eliminate the transient building response from consideration.

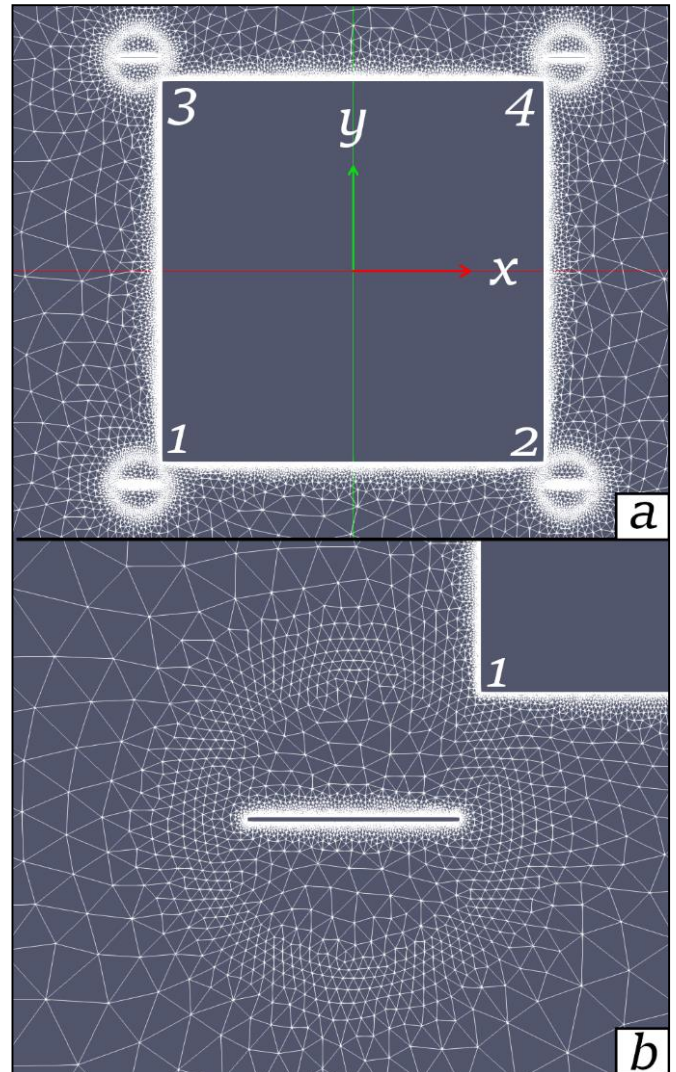


Fig. 4 Computational mesh for the building floor showing: (a) the whole building (b) details of plate 1

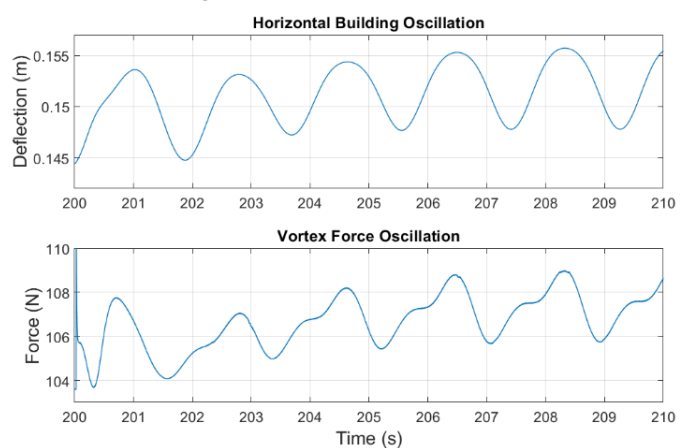


Fig. 5: Time history of building deflection vs. vortex-induced forces after matching

4.3 Amplitude Minimization

It is evidently straightforward to pick the best plate angle configuration for minimum amplitude from Fig. 6 or 7 for a specific wind speed. Figure 13 plots the best plate configuration for the range of speeds that were simulated. It can be noted that α_1 (for plates 1 and 3) appears to be more sensitive to changes in wind speed than α_2 . This is most likely due to the fact that plates 1 and 3 are on the windward side of the building thus significantly influencing flow for plates 2 and 4. It is also interesting to note that α_1 seems to prefer smaller angles around 45 to 70 degrees except for wind speed of 7.5 and 8 m/s. At these two speeds, α_1 jumps approximately 90 degrees while α_2 drops 90 degrees. The exact cause of this sudden angle swap is unknown and is currently undergoing further investigation.

4.4 Controller Development

A controller similar to the NACA0012 airfoil controller was developed for the 4-plate case. Instead of performing PID actions, however, a lookup table method was used for initial controller development. The lookup table relates wind speed to plate angles that were previously determined to reduce building motion based on simulation results. The controller simply consults this lookup table for the best plate configuration using a single-point reading of the wind velocity. A 60-second simulation for the building with the controller installed was performed. Table 2 lists the parameters that were assumed or calculated for the four-plate building. Figure 8 illustrates the response of the building equipped with 4 controllable plates. The wind speed is set at the inlet to 5 m/s. After the fluid domain stabilizes and the wind forces develop, a vibration of approximately 9.8 mm amplitude is observed in the figure. When the controller deploys the best angles for 5 m/s ($\pi/4$ and $7/8\pi$), the amplitudes diminish in approximately 7 seconds to 0.6 mm (94% reduction). The major reduction in vibration amplitudes is due mainly to the shifting of the wind force frequencies away from the natural frequency of the building. It should be noted that the 20 second delays are artificial and intended for the purpose of emphasizing the plate change effects.

Table 2: Parameters for the 4-plate building

Parameter	Value	Unit
Tuned Cantilever		
Height	30	m
Width	0.08	m
Depth	0.08	m
Density (ρ)	3.5	kg/m ³
Modulus (E)	1800	GPa
RE	50,000	-
CFD		
Width	1	m
Height	1	m
Depth	8	m
Plate length	0.1 (4 plate)	m
Plate length	0.03 (20 plate)	m
Air density (ρ)	1.225	kg/m ³
Wind direction	Positive x	-

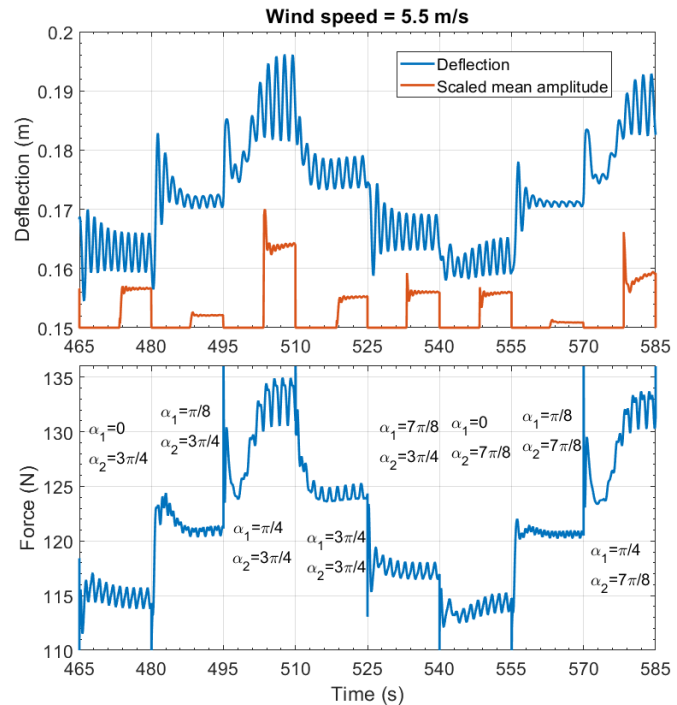


Fig. 6: Effect of plate angles on vortex-induced forces and building vibration amplitudes at 5.5 m/s wind speed

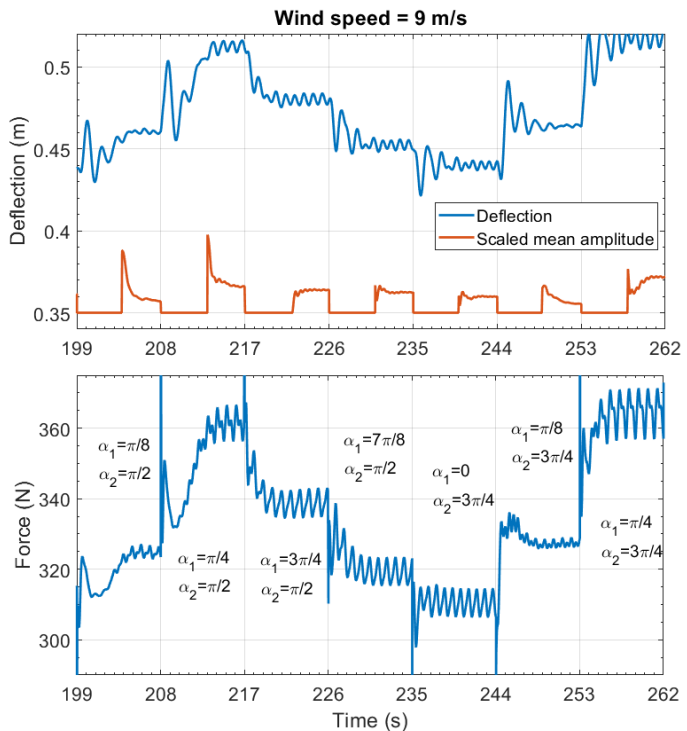


Fig. 7: Effect of plate angles on vortex-induced forces and building vibration amplitudes at 9 m/s wind speed

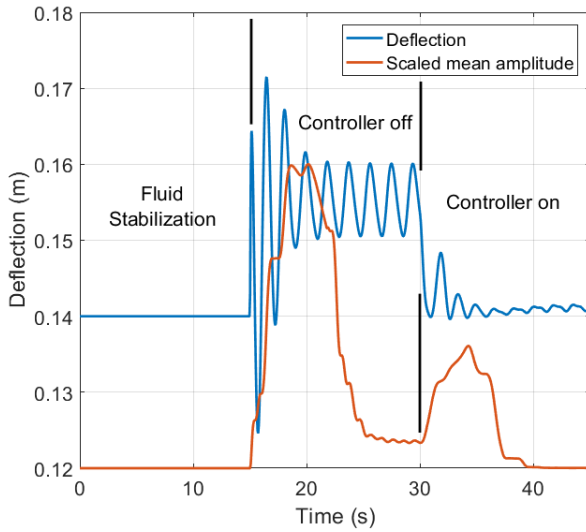


Fig. 8: Effect of controller action on the 4-plate building floor vibration amplitudes at 5 m/s wind speed

The primary advantage of a lookup table is efficiency. Given a wind speed, (and assuming the table contains accurate best plate angle data) the controller can immediately determine plate angles and begin positioning the plates without having to wait for feedback. While the lookup table control method demonstrates ability to mitigate wind-induced vibration, its oversimplification has limitations. Perhaps the most notable drawback of this method is the inability of the system to account for changes in building dynamics, and flow conditions. A potential solution to this drawback will be presented later in Section 4.6.

4.5 20-Plate Building

A real building façade will have plates that are smaller relative to the building than what was presented in the 4-plate building case. To investigate the feasibility of this work for larger deployments, the controller presented in the previous section was tested on a building surrounded by 20 smaller plates that discretize the former 4 plates. Figure 9 shows the mesh created for the 20-plate building case. The problem was again reduced to only two variables α_1 and α_2 by assuming symmetry around the x axis (wind direction is positive x) and by grouping neighborhoods of plates to have the same angle as illustrated in the figure. Figure 10 shows the behavior of the 20-plate building for the same simulation length as that used for the 4-plate cases. The performance of the controller does not seem to be greatly affected by the discretization of the large plates into smaller ones. This further underlines the feasibility of the system because grouping the plate angles into variables that represent a whole neighborhood enables the system to handle a much larger deployment capacity. The reduction of the vibration amplitude observed in Fig. 10 is 84% for 5 m/s wind speed. The amplitude reduction in this case is slightly inferior to the 4-plate case because the smaller plates do not change location, which means that their placement automatically assumes an angle that may not be desirable.

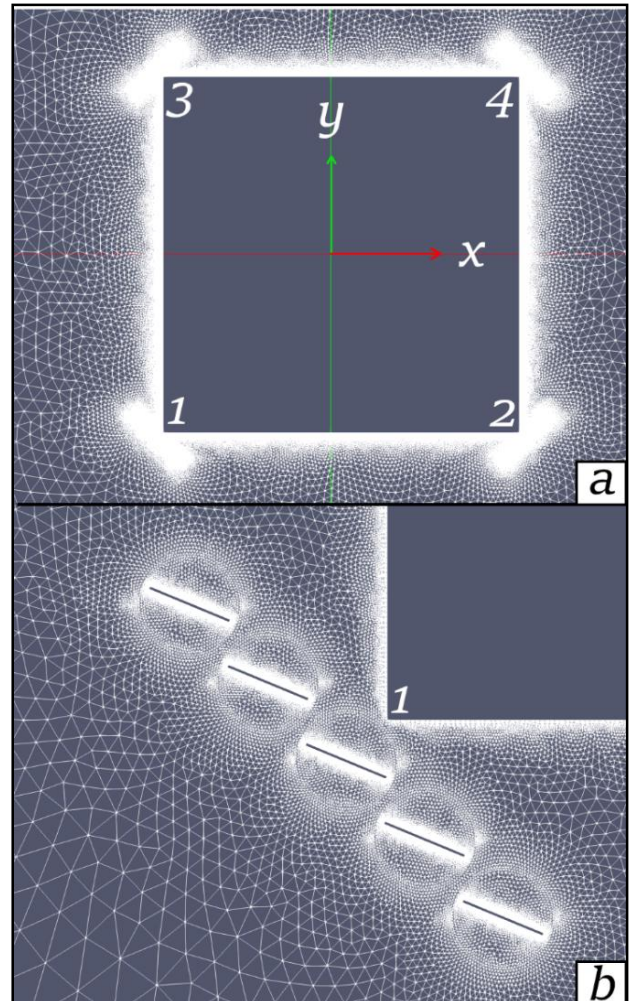


Fig. 9: Computational mesh for the 20 plate building floor
(a) top view of the floor (b) details of plate set number 1

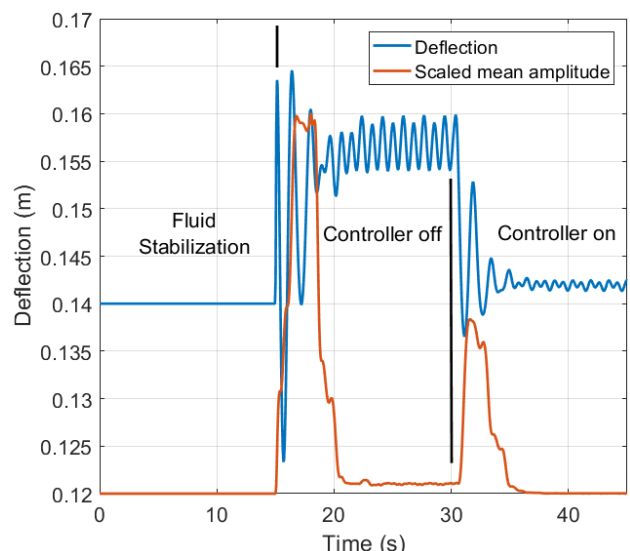


Fig. 10: Effect of controller action on the 20 plates building floor vibration amplitudes at 5 m/s wind speed

4.6 Artificial Neural Network Controller

The controller Section 4.4 considers only the wind speed v_w as an input to determine the best plate angle configurations. In reality, several other inputs and sources of variability play a significant role on the structural behavior of the building. The wind direction α_w is one of the factors that, in addition to being highly effective on its own, is especially important when combined with wind speed changes. Turbulence characteristics such as intensity and frequency content can also have a significant impact on building dynamics.

Also, the controller presented is based on a lookup table constructed from discrete plate angle changes (increments of $\pi/8$). Even though the table contains discrete angle data, the actual plate angles are continuous in reality. Furthermore, numerical interpolation of the behavior between the discrete angles may not be sufficiently reliable because of the highly variable nature of best plate angles for a given wind speed (recall Fig. 13). Considering all of this, a very large number of simulations that account for all possibilities is needed in order to design a reliable controller. Throughout the life of a building, environmental as well as structural changes occur that may considerably change its dynamic behavior, thus invalidating a predesigned controller. Floors could be remodeled or repurposed potentially altering mass distribution. The building façade may be redesigned for aesthetics or shading, thus altering aerodynamics. Other structures may be erected around the building effectively altering wind flow and turbulence characteristics. Any of these changes could significantly modify optimum plate configurations; therefore, a controller unable to adapt to these changes would become invalid.

The previous points strongly motivate the use of an ANN instead of a simple lookup table. With sufficient learning data, an ANN was shown to be able to generalize from previously encountered situations to unknown ones [16]. It can also use any current experience to update the internal weights that govern its regression to improve it [32], which gives it the ability to adapt to changes.

Figure 11 illustrates two ANNs that can be learned after the system has been deployed or in a wind-tunnel experiment of a building model, which significantly reduces the system design time by reducing the need for performing simulations. The readings of accelerometers mounted on the building can be integrated by a controller module to generate time series of building deflections [33]. A mean deflection amplitude (see Section 4.2) can then be calculated from this data for the current plate angles. The following steps illustrate the proposed learning process:

1. Using current data: Update ANN 1 (see Fig. 11) assuming mean amplitude \bar{A}_{new}
2. Using the current wind data alone: get the current best plate configuration from ANN 2
3. Using current wind data and the configuration obtained from step 2: obtain a mean deflection amplitude \bar{A}_{old} from ANN 1
4. if $\bar{A}_{old} > \bar{A}_{new}$: Update ANN 2 using the current plate configuration and wind data

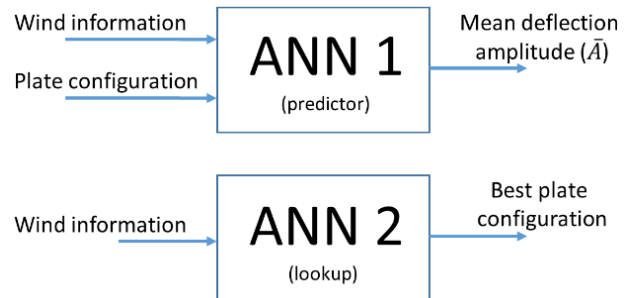


Fig. 11: Proposed ANN configuration for online learning

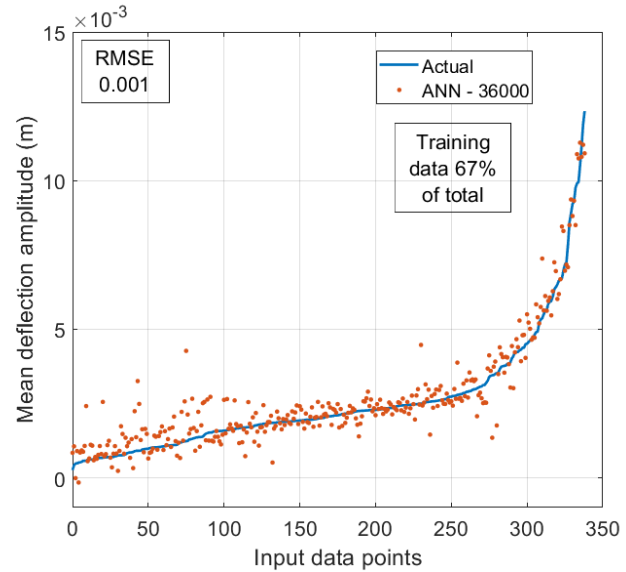


Fig. 12: ANN prediction of mean deflection amplitude after 36000 learning iterations

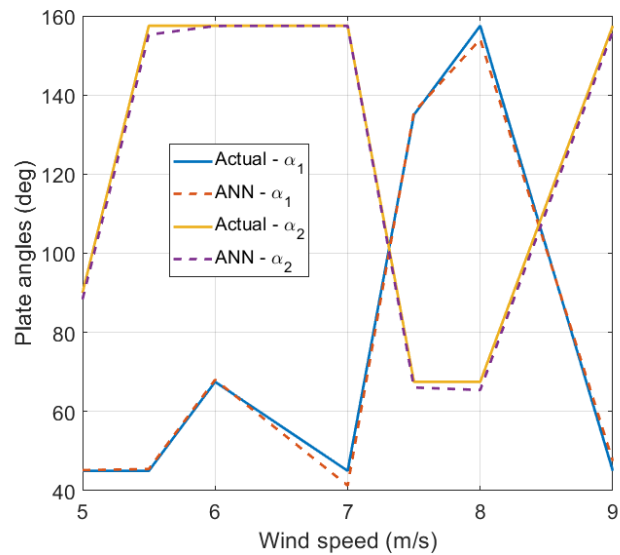


Fig. 13: ANN regression of best plate angles at different wind speeds after 16000 learning iterations

For a new deployment or experiment, the plate angles can be varied randomly or exhaustively in a systematic manner to effect the learning process. the ANNs can learn from an infinite number of data points for the length of the building's life, limited only by the frequency at which the learning procedure can occur. The controller needs only to consult ANN 2 to perform the plate angle changes.

An implementation of ANN 1 using only the velocity of the wind and two plate angles as inputs was created as a network of two hidden layers of 10 neurons with bipolar sigmoid activation functions. That specific setup was obtained using numerous trials. The network was learned using backpropagation on 67% of all the available wind speed, plate angles, mean amplitude combinations (~340 combinations). The learning was stopped when the network achieved sufficient prediction for the remaining 33% of the data set. Figure 12 plots the prediction of the network versus the actual data set. The prediction is in good agreement which justifies using the ANNs for the developed facade controller.

Similarly, an implementation of ANN 2 using a similar network setup was created from the best plate angle configurations previously obtained. Figure 13 shows a comparison of the best plate angle configurations between the ANN 2 implementation and the actual values for different wind speeds. The results are in good agreement but the prediction ability could not be demonstrated because the data set is relatively small (only 7 distinct speeds). Generating more data for ANN 2 is an ongoing effort of the research project, which will enable large-scale testing of the learning and control procedure.

6. SUMMARY AND CONCLUSIONS

The development of a smart façade controller to mitigate wind-induced vibrations in tall buildings was illustrated in this work. The preliminary design of the controller depends upon fluid-solid interaction simulations where forces from the fluid domain are applied on a solid frame representing the dynamic characteristics of the building. The simulation methodology was first validated using published data for the NACA0012 airfoil obtaining a good agreement. A building with 4 controllable plates attached to its corners was investigated at different plate angles and wind speeds. It was found that the plate angle variation shifts the frequency of the forcing vortex systems and considerably affects the amplitude of building vibrations. For each wind speed that was simulated, the best plate configuration was stored in a lookup table. A controller was developed which consults that lookup table using a point reading of the wind speed. The controller was found to reduce the amplitude of building vibrations by 94%. The controller was also tested for a building with 20 smaller plates which are grouped to act like 4 large plates. The performance of the controller was only slightly affected by this discretization, which proves the suitability of the system being developed for real-life building facades with a large number of plates. An ANN configuration that is suitable for online learning was presented and the preliminary results indicate the suitability of using ANNs as an adaptive replacement for the lookup tables.

ACKNOWLEDGMENTS

This research is funded by the National Science Foundation (NSF) award #1826364.

NOMENCLATURE

$\bar{\sigma}_{eff}$	Effective Cauchy stress tensor [Pa]
h	Rotational stiffness [N.m.s/rad]
Δt	Time step [s]
$C(c)$	Damping matrix (scalar damping) [N.s/m]
F	Force [N]
$K(k)$	Stiffness matrix (scalar stiffness) [N/m]
L	Lift force [N]
$M(m)$	Mass matrix (scalar mass) [kg]
U	Average velocity [m/s]
b	Rotational damping [N.m.s ² /rad]
j	Rotational inertia [N.m/rad]
k	Turbulence kinetic energy [J]
p	Average pressure [Pa]
α	Angle of attack [deg]
β	Damping matrix constant
ε	Turbulence kinetic energy dissipation rate [m ² /s ³]
ζ	Damping ratio
μ	Dynamic viscosity [m ² /s]
ν	Kinematic viscosity [m ² /s]
ρ	Density [kg/m ³]
τ	Torque [N.m]
ω	Rotational frequency [rad/s]
ϕ	Eigenvector

REFERENCES

- [1] A. A. Momtaz, M. A. Abdollahian and A. Farshidianfar, "Study of wind-induced vibrations in tall buildings with tuned mass dampers taking into account vortices effects," *International Journal of Advanced Structural Engineering*, vol. 9, pp. 385-395, 01 12 2017.
- [2] H. G. Poulos, "Tall building foundations: design methods and applications," *Innovative Infrastructure Solutions*, vol. 1, p. 10, 13 6 2016.
- [3] J. S. Love, T. C. Haskett and B. Morava, "Effectiveness of dynamic vibration absorbers implemented in tall buildings," *Engineering Structures*, vol. 176, pp. 776-784, 2018.
- [4] T. Sarpkaya, "A critical review of the intrinsic nature of vortex-induced vibrations," *Journal of Fluids and Structures*, vol. 19, pp. 389-447, 2004.
- [5] B. Cao and P. P. Sarkar, "Time-Domain Aeroelastic Loads and Response of Flexible Bridges in Gusty Wind: Prediction and Experimental Validation," *Journal of Engineering Mechanics*, vol. 139, pp. 359-366, 3 2013.
- [6] T. Kijewski-Correa and A. Bentz, "Wind-induced vibrations of buildings: role of transient events," *Proceedings of the Institution of Civil Engineers - Structures and Buildings*, vol. 164, pp. 273-284, 2011.

[7] J. D. Hobeck and D. J. Inman, "Artificial piezoelectric grass for energy harvesting from turbulence-induced vibration," *Smart Materials and Structures*, vol. 21, p. 105024, 8 2012.

[8] L. Micheli, A. Alipour and S. Laflamme, "Performance-Based Design for Wind-Excited Tall Buildings Equipped with High Performance Control Systems," 2018.

[9] A. Y. Tuan and G. Q. Shang, "Vibration control in a 101-storey building using a tuned mass damper," *Journal of Applied Science and Engineering*, vol. 17, pp. 141-156, 1 2014.

[10] A. Samanta and P. Banerji, "Structural vibration control using modified tuned liquid dampers," *The IES Journal Part A: Civil & Structural Engineering*, vol. 3, pp. 14-27, 2010.

[11] S. Gardarsson, H. Yeh and D. Reed, "Behavior of Sloped-Bottom Tuned Liquid Dampers," *Journal of Engineering Mechanics*, vol. 127, pp. 266-271, 3 2001.

[12] M. J. Tait, A. A. El Damatty, N. Isyumov and M. R. Siddique, "Numerical flow models to simulate tuned liquid dampers (TLD) with slat screens," *Journal of Fluids and Structures*, vol. 20, pp. 1007-1023, 11 2005.

[13] D. E. Rumelhart and J. L. McClelland, Parallel Distributed Processing: Explorations in the Microstructure of Cognition, The MIT Press, 1989.

[14] D. K. Jain, P. Shamsolmoali and P. Sehdev, "Extended deep neural network for facial emotion recognition," *Pattern Recognition Letters*, vol. 120, pp. 69-74, 2019.

[15] R. Ptucha, F. P. Such, S. Pillai, F. Brockler, V. Singh and P. Hutkowski, "Intelligent character recognition using fully convolutional neural networks," *Pattern Recognition*, vol. 88, pp. 604-613, 2019.

[16] T. Kim, O.-S. Kwon and J. Song, "Response prediction of nonlinear hysteretic systems by deep neural networks," *Neural Networks*, vol. 111, pp. 1-10, 2019.

[17] E. G. A. Antonini, D. A. Romero and C. H. Amon, "Improving CFD wind farm simulations incorporating wind direction uncertainty," *Renewable Energy*, vol. 133, pp. 1011-1023, 2019.

[18] T. Holzmann, Mathematics, Numerics, Derivations and OpenFOAM®, Holzmann CFD, 2016.

[19] B. E. Launder and D. B. Spalding, Lectures in mathematical models of turbulence, D. B. Spalding, Ed., Academic Press London, New York, 1972.

[20] D. Cabezón, E. Migoya and A. Crespo, "Comparison of turbulence models for the computational fluid dynamics simulation of wind turbine wakes in the atmospheric boundary layer," *Wind Energy*, vol. 14, pp. 909-921, 2011.

[21] W. P. Jones and B. E. Launder, "The prediction of laminarization with a two-equation model of turbulence," *International Journal of Heat and Mass Transfer*, vol. 15, pp. 301-314, 1972.

[22] A. Ribes and C. Caremoli, "Salome Platform Component Model for Numerical Simulation," in *Proceedings of the 31st Annual International Computer Software and Applications Conference - Volume 02*, Washington, 2007.

[23] H. G. Weller, G. Tabor, H. Jasak and C. Fureby, "A tensorial approach to computational continuum mechanics using object-oriented techniques," *Computers in Physics*, vol. 12, p. 620, 1998.

[24] U. Ayachit, The ParaView Guide (Full Color Version): A Parallel Visualization Application, Kitware, Incorporated, 2015.

[25] J. W. Banks, W. D. Henshaw, D. W. Schwendeman and Q. Tang, "A stable partitioned FSI algorithm for rigid bodies and incompressible flow in three dimensions," *Journal of Computational Physics*, vol. 373, pp. 455-492, 11 2018.

[26] A. S. Householder, "Unitary Triangularization of a Nonsymmetric Matrix," *Journal of the ACM*, vol. 5, pp. 339-342, 10 1958.

[27] M. A. Bhatti, Fundamental Finite Element Analysis and Applications: with Mathematica and Matlab Computations, Wiley, 2005.

[28] D. J. Inman, Engineering Vibration (4th Edition), Pearson, 2013.

[29] H. Jasak, "Dynamic Mesh Handling in OpenFOAM," in *47th AIAA Aerospace Sciences Meeting including The New Horizons Forum and Aerospace Exposition*, 2009.

[30] C. L. Ladson, "Effects of independent variation of Mach and Reynolds numbers on the low-speed aerodynamic characteristics of the NACA 0012 airfoil section," 1988.

[31] J. Moreno-Valenzuela, C. Aguilar-Avelar, S. A. Puga-Guzman and V. Santibanez, "Adaptive Neural Network Control for the Trajectory Tracking of the Furuta Pendulum," *IEEE Transactions on Cybernetics*, vol. 46, pp. 3439-3452, 12 2016.

[32] R. J. Vaccaro, M. Gindy, H. Nassif and J. Velde, "An Algorithm for Estimating Bridge Deflection from Accelerometer Measurements," in *2006 Fortieth Asilomar Conference on Signals, Systems and Computers*, 2006.